Applied Surface Science 420 (2017) 383–389

Contents lists available at ScienceDirect

Applied Surface Science

journal homepage: www.elsevier.com/locate/apsusc

Full Length Article

DFT study of methanol adsorption on PtCo(111)

V. Orazi[a,c], P. Bechthold[a,b], P.V. Jasen[a,b], R. Faccio[d], M.E. Pronsato[a,b], E.A. González[a,b,*]

[a] IFISUR (UNS-CONICET), Av. Alem 1253, (8000) Bahía Blanca, Argentina
[b] Departamento de Física, Universidad Nacional del Sur, Av. Alem 1253, (8000) Bahía Blanca, Argentina
[c] Departamento de Ingeniería Eléctrica y de Computadoras, Universidad Nacional del Sur, Av. Alem 1253, (8000) Bahía Blanca, Argentina
[d] Facultad de Química, Universidad de la República, Av. Gral. Flores 2124, C.C. 1157, (11800) Montevideo, Uruguay

ARTICLE INFO

Article history:
Received 8 March 2017
Received in revised form 23 April 2017
Accepted 18 May 2017
Available online 23 May 2017

Keywords:
DFT
PtCo
Methanol
Adsorption
Bonding

ABSTRACT

Methanol adsorption on PtCo(111) surface at low coverage is studied using Density Functional Theory (DFT) calculations without and with van der Waals corrections. We investigated the PtCo FCT alloy surface with a uniform distribution. The most favorable site for CH_3OH adsorption is on top of a Co atom, with an adsorption energy of −0.92 eV. Methanol attachs to the surface by the O atom, with a distance of 2.24 Å. The molecule presents a small distortion after adsorption. The C—O—Co bond angle is 142°. The C—H bonds are strengthened whereas the C—O and O—H bonds are weakened. A charge transfer from C atom to O atom occurs upon adsorption, and then further transfer occurs to the Co atom on the surface. The calculated vibrational frequencies for adsorbed methanol present a red-shift displacement compared to gas-phase, confirming the adsorption process.

1. Introduction

Gas adsorption on surfaces has attracted much attention among physicists and chemists for most of this century [1]. The research efforts in this matter have provided unprecedented advances in the fundamental principles that control electrocatalytic reactions; and applications in fuel cell science where the chemical energy, stored in materials such as primary alcohols (methanol and ethanol), can be electrochemically converted in electricity [2].

The use of methanol (CH_3OH) as fuel presents several advantages in comparison to hydrogen: it is a cheap liquid fuel, easily handled, transported, and stored; with a high theoretical energy density [3–5]. In addition, the methanol is the simplest alcohol than can be understood as a construction of C—H, C—O and O—H bonds; with a relatively high complexity so that it can be used as a good model for understanding the chemical bond properties of more complex gases [1,4]. The interest of researchers in fuel cells increases from year to year because fuel cells offer a cleaner and more efficient source of energy when compared with other energy-conversion devices. In the early days, research in the field of fuel cells addressed fundamental aspects, but now the emphasis has shifted from fundamental to technological applications [6].

Fuel cells are electrochemical devices in which both fuel and oxidant are fed in a continuous supply to the electrodes. In general, they require electrocatalysts at the anode to oxidize the fuel to produce electrons and protons and at the cathode to reduce oxygen and consume the protons and electrons produced. They are attractive sources of electrical power since the production of electrical energy can be maintained as long as the reactants are supplied to the electrodes [1,2,7,8].

Compared to traditional power sources, fuel cell technology is a favorable energy source for a myriad of reasons. It presents low environmental impact, high electric conversion efficiency for different systems (35–70%), independence of size, reliability and long lasting operation, production of heat that is usable for co-generation cycles, and the flexibility of the utilized fuel. Besides, unlike most rechargeable power sources for portable electronic devices, such as state-of-the-art lithium-ion batteries, the amount of time required to recharge a depleted methanol fuel cell is virtually zero. Among all kinds of fuel cells, direct methanol fuel cells (DMFC) have really exhibited potentialities to replace current portable power sources and micro power sources in the market, like lithium-ion batteries [9 and ref. therein].

The performance of DMFCs is limited due to the presence of various drawbacks, including kinetics constraints and catalyst poisoning. In a DMFC, methanol is oxidized to carbon dioxide and water. Methanol oxidation is a slow reaction that requires active sites for the adsorption of methanol [10].

* Corresponding author at: Departamento de Física, Universidad Nacional del Sur, Av. Alem 1253, (8000) Bahía Blanca, Argentina.
E-mail address: egonzal@uns.edu.ar (E.A. González).

http://dx.doi.org/10.1016/j.apsusc.2017.05.159
0169-4332/

Low temperature fuel cells, such as the polymer electrolyte membrane fuel cells (PEMFC) and the DMFC, utilized platinum or platinum alloys as electrode materials. Platinum possesses the highest catalytic activity and therefore it has been widely used in most fuel cell systems [6].

The methanol utilized as fuel in the DMFCs offer direct conversion to electricity, without any auxiliary process for intermediating fuel processing or fuel reforming steps, which are required in others FCs, e. g. hydrogen PEM fuel cells (H_2-PEMFC) [1,9,11].

The methanol adsorption, and its decomposition products, on transition metal surfaces has been extensively investigated, one example involves platinum surfaces and Pt-modified metals. Pt is the most active metal, in acid medium, for methanol electrooxidation. However, the poor abundance and high cost limit commercial applications. Additionally, the Pt performance is far from acceptable for their use as electrode in DMFCs. One solution is the alloying of Pt with cheaper 3-d metals, such as Fe, Co, and Ni; these alloys are found to have comparable, and even better, catalytic activity under PEM-FC operating conditions [11 and ref. therein]. In this sense, bimetallic electrocatalysts such as PtRu, PtSn, PtCo or PtNi are more tolerant to CO poisoning, and the methanol electrooxidation reaction starts at less positive potentials than bare-Pt [10 and ref. therein].

In particular, the Pt-Co alloy has been used for multiple purposes, because of its interesting magnetic and catalytic behavior [12–16]. The Co improve the methanol oxidation reaction (MOR) of the electrocatalyst due to the lowering of the electronic binding energy, which promotes the C—H cleavage reaction at low potentials. In one hand, the presence of cobalt oxides provides the required oxygen for the CO oxidation at lower potentials. On the other hand, a higher methanol-tolerance is expected for the Pt–Co alloy catalysts, in comparison to bare Pt, ascribed to the dilution effect of Pt and thus hindering the methanol adsorption. Furthermore, this alloy presents an improved activity for the oxygen reduction than pure Pt [5].

The adsorption of the CH_3OH on PtCo alloys has been experimentally studied [5,10,17], but to the best of our knowledge there are no theoretical works on PtCo(111) surface. However, there are several theoretical studies of methanol adsorption on pure metal surfaces or clusters and on others bi-metallic alloys surfaces, among them studies on Pt [1,18,19], Co [20,21], Pd [22,23], Cu [23–25], Ru [26], Ni [27], Au [28], Co/Pt(111) [29], PtRu [1], PdZn [30], PdIn [31], AuPd [32] and PtAu [33].

In this work, we performed *First Principles* calculations using Density Functional Theory (DFT) to evaluate the stability of methanol adsorption on a PtCo alloy. The changes in the electronic structure, chemical bonding, including the bond orders implemented in DDEC6 method [34–36], and vibrational frequencies after adsorption were also studied.

2. The surface model and the computational method

The crystal structure of the PtCo alloy presents two-phases. A chemically disordered face centered cubic (FCC) phase (space group Fm-3m) [37,38], which correspond to the low temperature structure, and a structurally ordered $L1_0$ or face-centered tetragonal (FCT) structure for the high temperature regime [37,38]. In this work, we have modeled this last one structure that presents a crystal space group P4/mmm [37,38]. The reason for that choice is that under operation condition, in fuels electrodes, the high temperature phase is the most stable as reported by Stassi et al. [39]. These authors proved that the catalyst, characterized as a disordered FCC structure, performed slightly better at low temperatures (80 °C) and full humidification. Moreover, the primitive cubic ordered structure catalyst showed superior characteristics in terms of performance due to its stability at high temperature (110 °C) and at low relative humidity. These last operating conditions are very relevant for automotive applications.

The calculated *a* and *c* lattice parameters for PtCo FCT bulk are 3.81 and 3.71 Å, respectively. These values are in good agreement with the experimental data (3.78 and 3.71 Å, respectively) [40] and from literature values [11,41]. We selected the (111) crystallographic plane to study the methanol adsorption because we found it was the most stable surface, in coincidence with previous calculation of Hirunsit and Balbuena [11] and Dannenberg et al. [42]. In the next sections, we will consider the computational methodology and the adsorption models.

2.1. Computational method

The first principles calculations based on spin polarized Density Functional Theory (DFT) were performed using the Vienna Ab-initio Simulation Package (VASP), which employs a plane-wave basis set and a periodic supercell method [43–45]. The Kohn-Sham equations with periodic boundary conditions were solved variationally using the projector-augmented wave (PAW) method [46,47]. The exchange and correlation energies were calculated with the Perdew-Burke-Ernzerhof form of the spin-polarized generalized gradient approximation (GGA-PBE) [48].

For the plane wave basis set expansion a kinetic energy cutoff of 300 eV was used for all calculations, overall with the gamma-centered Monkhorst-Pack scheme of $7 \times 7 \times 1$ k-points grid for integration over the Brillouin zone [49]. The tolerance for the geometry optimization was set to a force of 0.02 ev/Å and a total energy difference down to ~1 meV/atom. Equilibrium lattice constants of 3.81 and 3.71 Å were selected, as obtained in a previous work [50].

The Grimmeís DFT-D2 method was adopted to account for the van der Waals interaction (vdW), which is optimized for several DFT functional [51].

We defined the stabilization energy PtCo-CH_3OH with respect to isolated atoms as following:

$$\Delta E_{ads} = E_{ads}(CH_3OH/PtCo) - E_{Total}(PtCo) - E_{Total}((CH_3OH)_{molec}) \quad (1)$$

where E_{Total} $((CH_3OH)_{molec})$ is the energy of the isolated methanol molecule and E_{Total} $(PtCo)$ is the total energy of the clean surface alloy supercell.

DFT-D2 method considers the total energy (E_{Total}) as the sum of two terms shown in Eq. (2),

$$E_{total} = E_{KS} + E_{vdW} \quad (2)$$

where, E_{KS} and E_{vdW} are Kohn-Sham and van der Waals energies respectively. Taking into account Eq. (2), it is easy to separate the adsorption energies into two contributions [51], expressing the adsorption energy as the sum of the chemical adsorption energy and the dispersive adsorption energy,

$$E_{ads(Total)} = E_{ads\text{-}KS} + E_{ads\text{-}vdW} \quad (3a)$$

$$E_{ads(KS)} = E_{KS}(CH_3OH/PtCo) - E_{KS}(PtCo) - E_{KS}(CH_3OH) \quad (3b)$$

$$E_{ads(vdW)} = E_{vdW}(CH_3OH/PtCo) - E_{vdW}(PtCo) - E_{vdW}(CH_3OH) \quad (3c)$$

here $E_{ads(KS)}$ and $E_{ads(vdW)}$ are the adsorption energies calculated with Kohn-Sham energies, and with dispersion energies corresponding to vdW interactions. In this way, the nature of the bonding can be appreciated through these total energies.

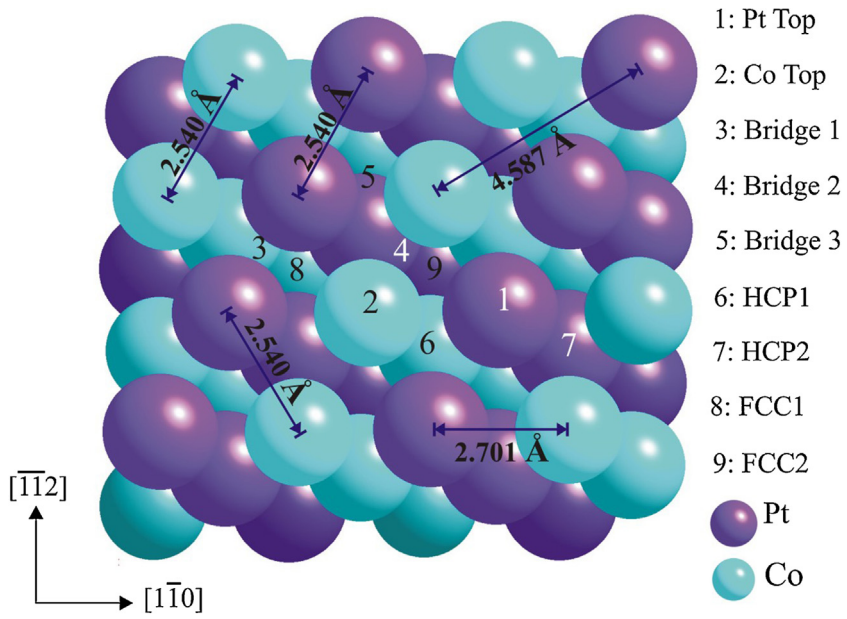

Fig. 1. Schematic top view of the PtCo(111) surface alloy. The high symmetry adsorption sites are indicated. The grading in colors indicates the different and more inner layers. The distances indicate corresponding to the surface alloy without relaxations.

In order to understand the CH_3OH/PtCo interactions and bonding we used the concept of Density of States (DOS) and the overlap population (OP) [52,53]. Additionally, we computed the electronic charges on atoms using Bader analysis [54], Bond Order (BO) as implemented in the DDEC6 method [34–36] and finally we determined the corresponding vibrational frequencies.

2.2. The (111) surface and adsorption models

In a previous work, we calculated the stability of the ordered atomic planes (001), (100), and (111) in FCT PtCo structure [50,55]. The most stable plane of PtCo FCT result to be the (111), in agreements with previous calculations of Hirunsit and Balbuena [11] and Dannenberg et al. [42]. We must point out that the results of the later study do not addressed the alloy surface stability, which can be determined using surface free energy and surface segregation energy as recently reported [32].

We represented the (111) plane with a supercell. The schematic top view of the PtCo(111) is shown in Fig. 1, where all the possible adsorption sites and the metal–metal bond distances prior relaxation are indicated. In order to achieve the best compromise between computational time and accuracy of our model, we selected a seven layers slab separated in the [111]-direction by a vacuum region. The vacuum distance of 6 top layers (>13 Å) was enough to avoid spurious interaction between periodic configurations. The thickness of PtCo(111) slab should be such that it approaches the electronic structure of 3D bulk PtCo in its innermost layer.

When considering methanol adsorption on the PtCo(111) surface at low coverage (1/16 ML), the molecule-surface distance was optimized allowing to relax the first three layers of the metal slab until reaching a 1 meV convergence in the total energy; the four remaining layers (bulk like) were kept fixed. We studied the molecular adsorption at all the high symmetry sites on the (111) surface and we determined the most stable site for adsorption (see Figs. 1 and 2). For the sake of clarity, Figs. 1 and 2 only shows the first three layers of the slab.

3. Results and discussion

Table 1 lists the adsorption energy, distances between atoms from methanol molecule after adsorption and the oxygen height over surface (h) for all the high symmetry sites. In this Table can be seen that methanol adsorption at low coverage on PtCo(111) surface alloy is a favorable process in almost all high symmetry, except in the case of bridge1 site. The most stable situation is at

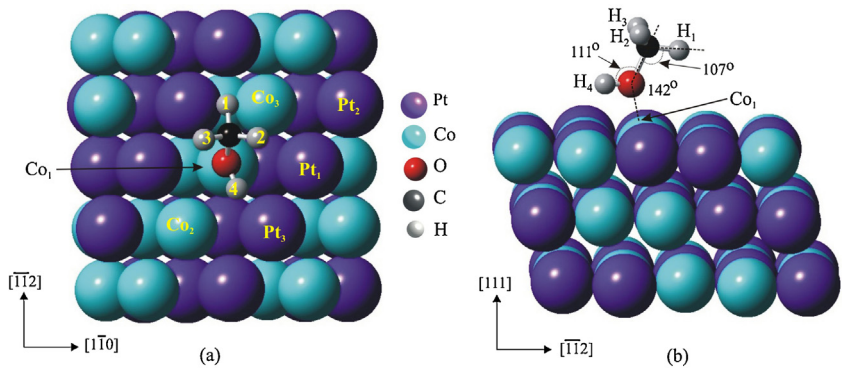

Fig. 2. Schematic view of the CH_3OH/PtCo(111) surface after molecule adsorption: (a) top view where OP geometry is indicated; and (b) lateral where the C—H, C—O—H and C—O—Co angles are indicates. The grading color indicates the inner layers.

Table 1
Adsorption Energy of methanol molecule on PtCo(111) surface alloy[a], distances between atoms after adsorption and O height over surface (h) for the high symmetry adsorption sites. The geometry is shown in Fig. 1.

Site	Bridge1	Bridge2	Bridge3	FCC1	FCC2	HCP1	HCP2	Top Co	Top Pt
E_{ads} (eV)	−0.35 (−)	−0.48 (−0.06)	−0.69 (−0.12)	−0.59 (−0.08)	−0.42 (−0.02)	−0.40 (−0.03)	−0.50 (−0.06)	−0.92 (−0.23)	−0.45 (−0.05)
h (Å)	2.704	2.549	2.289	2.441	2.686	2.578	2.657	2.238	2.563
$d_{O\text{-}C}$ (Å)[b]	1.432	1.440	1.446	1.440	1.438	1.438	1.433	1.444	1.440
$d_{O\text{-}H4}$ (Å)[b]	0.980	0.977	0.983	0.985	0.981	0.979	0.984	0.979	0.979
$d_{C\text{-}H1}$ (Å)[b]	1.097	1.097	1.097	1.097	1.100	1.096	1.097	1.096	1.097
$d_{C\text{-}H2}$ (Å)[b]	1.103	1.102	1.101	1.102	1.100	1.102	1.103	1.101	1.100
$d_{C\text{-}H3}$ (Å)[b]	1.102	1.102	1.100	1.101	1.100	1.102	1.103	1.100	1.101

[a] Numbers in parentheses are without vdw corrections.
[b] Molecular distances in vacuum: $d_{O\text{-}C}$ = 1.44 Å, $d_{O\text{-}H4}$ = 0.97 Å, $d_{C\text{-}H}$ = 1.10 Å.

the Top site on a Co atom with an adsorption energy of −0.23 eV (see Table 1 and Fig. 2). This value is similar to those reported on Co(0001) and Co(111) [20] and smaller than that on Pt(111) [18], whose values are −0.23, −0.22 and −0.33 eV, respectively. For all mentioned cases, the adsorbed molecule prefers to bind to the on-top site through its oxygen atom at the surface. To evaluate the effect of dispersion forces in the total energy value for all site we included van der Waals corrections. In those cases all high symmetry adsorption sites are stables. The trend of energies values is the same with or without vdW corrections. The energy value for the most stable site, Top site on a Co atom, is −0.92 eV that is in good agreement with that reported by Skoplyak et al. [42]. These authors obtained by DFT calculation an adsorption energy of ∼−1.2 eV for CH_3OH on Co-Pt-Pt(111).

Methanol attachs to the surface through the oxygen atom, with a distance of 2.24 Å. This distance is very similar to that reported on Pt(111) [18,19], Co(0001) [20], PtRu [1,26], PdIn(111) [31] and PtAu [33]. The C—O—Co bond angle decrease from 180° to 142°, facilitating the binding of methanol to the surface via the oxygen lone-pair orbital (see Fig. 2b). The adsorbate presents a small distortion after adsorption. The bond lengths for C—O, C—H and O—H are calculated to be 1.444, 1.096 and 0.979 Å, which are close to the molecular distance in vacuum (see Table 2). The Co_1 atom (Co atom just below the molecule) presents a slightly displacement outward the surface after adsorption. Two H atoms from the methyl group pointed forward the surface meanwhile the third H pointed towards. The H—C—O bond angles change from 106° to 107° (H towards) and to 110° (H forward) (see Fig. 2b). Greely and Mavrikakis [19] report this same possible adsorption geometry for CH_3 group on Pt(111). The C—O—H bond angle is about 111° whereas initially is of 108° (see Fig. 2b).

The electronic structure study was performed to understand the process of methanol adsorption on PtCo(111). Bond order (BO), overlap population (OP) and their percentage change with respect to clean surface are listed in Table 2. The final adsorption geometry and atoms involved in the OPs are indicates in Fig. 2.

We can see from Table 2 that Co–Co bonds lengths have a small increment after methanol adsorption. Similar behavior present the Pt-Co distances except for Pt_1—Co_1, which is shortened after adsorbate interaction because of the increment presented on Co_1—Co_2 and the Co_1 atom movement. On the other hand, the Pt–Pt bond lengths do not present significative changes.

Table 2
Bond Order (BO), overlap population (OP) and OP percentage change with respect to clean surface (ΔOP%) for CH_3OH/PtCo(111) before and after molecular adsorption. The geometry is shown in Fig. 2.

Bond	OP			BO			Distances (Å)	
	before	after	ΔOP%	before	after	ΔBO%	before	after
$Pt_1 \leftrightarrow Pt_2$	0.578	0.580	0.3	0.830	0.834	0.5	2.540	2.539
$Pt_1 \leftrightarrow Pt_3$	0.578	0.575	−0.5	0.830	0.827	−0.4	2.540	2.541
$Co_1 \leftrightarrow Co_2$	0.291	0.264	−9.3	0.325	0.279	−14.1	2.538	2.571
$Co_1 \leftrightarrow Co_3$	0.297	0.261	−12.1	0.325	0.276	−15.1	2.541	2.550
$Pt_1 \leftrightarrow Co_1$	0.293	0.258	−11.9	0.320	0.273	−14.7	2.799	2.764
$Pt_1 \leftrightarrow Co_3$	0.408	0.396	−2.94	0.509	0.489	−3.9	2.583	2.591
$Pt_2 \leftrightarrow Co_3$	0.293	0.293	0	0.320	0.319	−0.3	2.801	2.807
$Pt_3 \leftrightarrow Co_1$	0.408	0.364	−10.8	0.509	0.436	−14.3	2.584	2.600
$Pt_3 \leftrightarrow Co_2$	0.293	0.294	0.3	0.320	0.320	0	2.802	2.873
$O \leftrightarrow C$	0.803	0.737	−8.2	1.452	1.275	−12.2	1.429	1.444
$O \leftrightarrow H_1$	0.033	0.035	6.1	0.044	0.037	−15.9	2.035	2.057
$O \leftrightarrow H_2$	0.028	0.028	0	0.038	0.029	−23.7	2.110	2.102
$O \leftrightarrow H_3$	0.025	0.028	12.0	0.038	0.029	−23.7	2.110	2.091
$O \leftrightarrow H_4$	0.552	0.466	−15.6	0.826	0.652	−21.1	0.972	0.979
$C \leftrightarrow H_1$	0.560	0.549	−2.0	0.843	0.834	−1.1	1.098	1.096
$C \leftrightarrow H_2$	0.578	0.555	−4.0	0.872	0.849	−2.6	1.105	1.100
$C \leftrightarrow H_3$	0.578	0.555	−4.0	0.873	0.848	−2.9	1.105	1.101
$C \leftrightarrow H_4$	0.038	0.040	5.3	0.043	0.041	−4.6	1.963	2.010
$Pt_1 \leftrightarrow O$	–	0.041	–	–	0.041	–	–	3.698
$Pt_3 \leftrightarrow O$	–	0.046	–	–	0.045	–	–	3.198
$Pt_3 \leftrightarrow H_4$	–	0.080	–	–	0.080	–	–	2.682
$Co_1 \leftrightarrow O$	–	0.535	–	–	0.810	–	–	2.238
$Co_1 \leftrightarrow C$	–	0.012	–	–	0.012	–	–	3.492
$Co_1 \leftrightarrow H_4$	–	0.124	–	–	0.137	–	–	2.631
$Co_2 \leftrightarrow O$	–	0.033	–	–	0.032	–	–	3.119
$Co_2 \leftrightarrow H_4$	–	0.057	–	–	0.058	–	–	2.949
$Co_3 \leftrightarrow O$	–	0.039	–	–	0.039	–	–	3.855

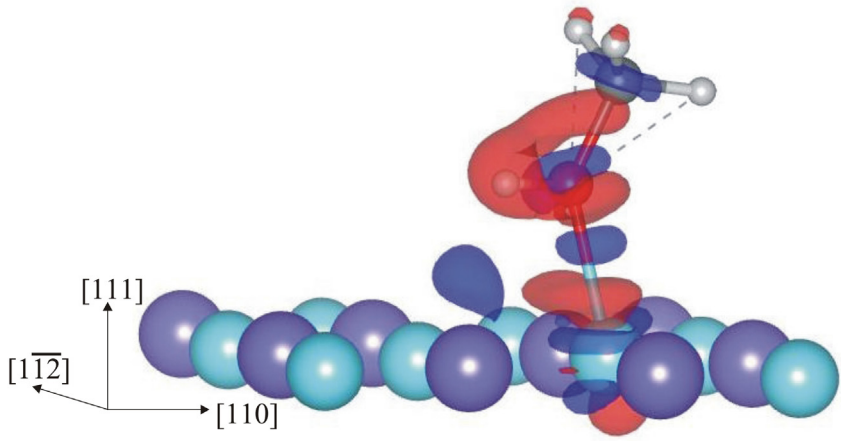

Fig. 3. Charge distribution view around methanol adsorbed on PtCo(111). Red color indicates positive charge and blue negative charge. (For interpretation of the references to colour in this figure legend, the reader is referred to the web version of this article.)

The BO of Pt–Pt bonds do not present noticeable changes after adsorption, which are consistent with almost no change in their distances and their electronic charges. The most important change in BO occurs for Pt_3 with a 2.6% (from 4.318 to 4.429); however, total BO for Pt_1 change from 4.316 to 4.304 (−0.3%). On the other hand, BO of metal-Co bonds present changes around −14%. The Co—Co BO decrease −14.1% and −15.1% for Co_1—Co_2 and Co_1—Co_3, respectively. The BO Pt-Co bonds decrease about −14.7% for Pt_1—Co_1 and −14.3% for Pt_3—Co_1 meanwhile Pt_1—Co_3 only decrease in about −4.0%. The mayor change corresponds to Co_1 whit about 19% (from 3.053 to 3.636) meanwhile Co_3 experiment a reduction of its total BO of only about −1.4% (from 3.053 to 3.009).

Considering the atoms from methanol molecule, the total BO for O change from 2.399 to 3.093 (28.9%), C from 4.083 to 3.890 (−4.7%), H_1 from 0.936 to 0.926 (−1.1%), H_2 from 0.965 to 0.934 (−3.0%), H_3 from 0.965 to 0.936 (−3.2%) and H_4 (H from O—H) from 0.879 to 1.002 (+14.0%). All atom-atom BO from the molecule adsorbed decrease after adsorption, which is consistent with an elongated bond distances. In the case of the adsorbate-substrate bonds, the most significative BO changes correspond to the Co_1—O and Co_1—H_4 with 0.810 and 0.137, respectively (see Table 2).

The Bader charge difference was computed for CH_3OH/PtCo system. The most affected atoms are Co_1, O and C atoms with a change of 32.0% (from −0.415 to −0.548), 45.0% (from 1.175 to 1.706) and −14.0% (from −0.670 to −0.571) respectively. The H_4 (OH bond) present a small change (0.3%) and the H atoms bonded to C do not show relevant charge differences.

The BO reduction (increase) of a particular atom-atom bond is linked to the bond elongated (shortened) distance. The decrease in the atom total BO value corresponds to a negative Baderís charge difference percentage; that is, the atom electronic charge density decreases in reference to its initial value.

Similar consideration about bonding can be seen from changes in the OP. The main result is that the methanol adsorption modifies the overlap population for the surface atoms nearby the adsorbate final location (see Table 2).

Fig. 3 shows the electron density distribution of the methanol adsorbed on the most favorable site. The charge density difference ($\Delta\rho$) isosurface is calculated using the following expression:

$$\Delta\rho = \rho(CH_3OH/PtCo) - \rho(CH_3OH) - \rho(PtCo)$$

where ρ(PtCo) is the charge density of the relaxed surface and $\rho(CH_3OH)$ is that one of the adsorbed molecule. In this figure it can be seen that the transferred charge between adsorbate and substrate is consistent with Bader difference charge and previous BO analysis. So, the charge transfer seems to occur from C atom to O atom and then to the Co_1 atom (surface).

Fig. 4 shows the DOS plots before and after methanol adsorption. The Total DOS curves (see Fig. 4a) present small peaks at −22.3, −13.0 and −8.7 eV coming from the interaction with methanol. The region near the Fermi level shows a not uniform spin density distribution, which is an indication of the magnetic nature of the surface. The d-band of the metallic surface appears to be wider after adsorption (see Fig. 4a). The PDOS curves for Pt and Co atoms do

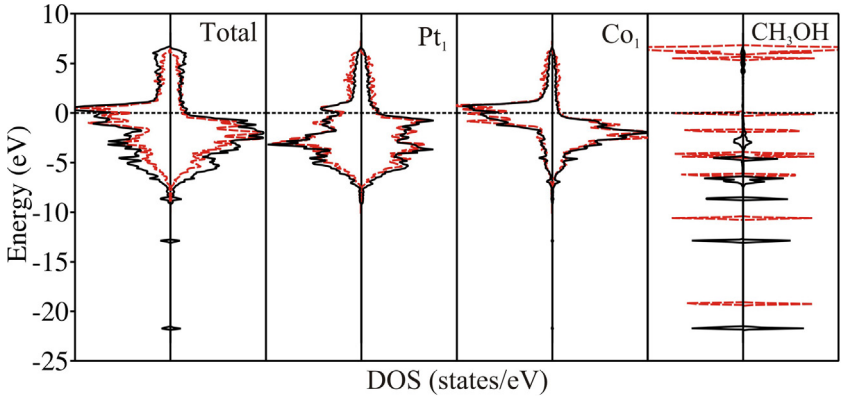

Fig. 4. DOS curves for the CH_3OH/PtCo(111) before and after molecule adsorption. (a) Total, (b) projected on Pt atom from surface, (c) projected on Co atom and (d) projected DOS curves for the methanol molecule. The dashed red line indicates the curve before molecule adsorption. (For interpretation of the references to colour in this figure legend, the reader is referred to the web version of this article.)

Table 3
Vibrational frequencies of methanol (in cm^{-1}). (The nomenclature used is the same that in Ref. [57]).

	CH3OH (g)[a] Exp.	Pt(111) top[b] HREELS	Ru(0001)top[c] GAUSSIAN	Vacuum VASP	TOP Co VASP
ν(O—H) —stretch—	3510	3714	3669.1	3832.1	3582.0
$\nu(CH_3)$ —stretch—	2994	3101	3035.8	3063.6	3087.2
	2969	3067	2983.1	2998.5	3036.6
	2926	2989	2920.6	2942.0	2971.1
	2822				
$\delta_{as}(CH_3)$ —bend—	1454	1426	1452.6	1456.7	1452.1
			1440.8	1445.1	1440.5
$\delta_s(CH_3)$ —bend—			1403.4	1420.5	1418.3
$\nu(CH_3OH)$ in phase	1304	1274	1289.9	1315.6	1287.5
$\nu(CH_3OH)$ out of plane			1123.8	1130.1	1130.7
$\nu(CH_3OH)$ out of phase	1061	1057	1030.1	1045.8	1049.9
ν(CO) —stretch—	975	961	981.6	988.8	982.6
ν(Co—O)	–	–	–	–	190.1

[a] Taken from Ref. [56].
[b] O—bond, one methyl H toward surface taken from Ref. [19].
[c] Taken from Ref. [57].

no present significative changes after adsorption except for small peaks located at −22.3, −13.0 and −8.7 eV on PDOS for Co (see Fig. 4b and c). Fig. 4d shows the CH_3OH PDOS curve before and after adsorption. The shift of the black curve to lower energies indicates that methanol molecule is stabilized after adsorption. From Fig. 4c and d it can be seen that the adsorbate-surface interaction is mainly through the Co atom located just below the molecule. In addition, the concentration of charge around the hydroxyl group and Co_1 in Fig. 3 is consistent with the hybridization shown in Fig. 4.

Finally, vibrational frequencies for methanol and O—Co bond are given in Table 3. The agreement between the experimental data [56] and the calculated for methanol in this top configuration is quite good. The calculated vibrational frequencies for adsorbed methanol are similar to those reported for Pt(111) [19] and Ru(0001) [57] in top configuration. The calculated bands at 1287–1452 cm^{-1} correspond to the C—H bending modes, while those in the range 2971–3582 cm^{-1} correspond to C—H and O—H stretching bands. The vibrational mode located at 983 cm^{-1} corresponds to the C—O stretching mode in methanol. The 1050–1287 cm^{-1} bands correspond to the mixed bending modes that consider the vibrational motion on no parallel to the methanol symmetry plane (out of plane) and in phase and out of phase. The Co—O calculated frequency is 250 cm^{-1}, which is similar with the reported by Bigotto et al. [58]. All the determined vibrational frequencies for methanol present a red shift compared to the gas-phase.

4. Conclusions

We investigated the methanol adsorption on PtCo(111) surface with an uniform distribution of metallic atoms. Co Top site is the most stable adsorption position with an adsorption energy of −0.92 eV. The molecule is adsorbed at a distance of 2.24 Å over the surface and it presents a small distortion after adsorption. The C—O—Co bond angle is 142° and the C—O—H bond angle is about 111°. The C—O and O—H bonds show a small elongation whereas the C—H bonds are shortened.

BO metal-Co bonds present changes around −14%. The mayor total BO change for Co atoms corresponds to Co_1 but Co_3 experiment a reduction of its total BO. The total BO for O atom and for the H bonded to it increase 28.9% and 14.0%, respectively.

The methanol adsorption modifies the overlap population from the surface atoms nearby the adsorbate in its final location. A charge transfer from C atom to O atom and then to the Co_1 atom on the surface is predicted from computational calculations and can be seen in Fig. 3.

The main result of this work is that the interaction of methanol with a PtCo surface is favorable. The changes of the C—O and O—H bond distances and the C—O—Co bond angle upon adsorption, thus constituting that the CH_3OH adsorption on PtCo(111) is not very strong and required the inclusion of van der Waals corrections.

Acknowledgements

Our work was supported by ANPCyT through PICT2014-1351 and PIP-CONICET PIP 2014–2016 code: 11220130100436CO research grants, as well as by SGCyT-UNS. P.B., P.V.J., M.E.P. and E.A.G. are members of CONICET. V.O. is a fellow researcher at that Institution. RF acknowledge PEDECIBA, CSIC and ANII, Uruguayan Institutions.

References

[1] W.T. Cahyanto, A.A.B. Padama, M.C.S. Escaño, H. Kasai, Preferential sites for adsorption of methanol and methoxy on Pt and Pt-alloy surfaces, Phys. Scr. 85 (2012) 0156051/1–0156051/6.
[2] B. Braunchweig, D. Hibbitts, M. Neurock, A. Wieckowski, Electrocatalysis a direct alcohol fuel cell and surface science perspective, Catal. Today 202 (2013) 197–209.
[3] J.H. Meng, C.A. Menning, M.B. Zellner, J.G. Chen, Effects of bimetallic modification on the decomposition of CH_3OH and H_2O on Pt/W(110) bimetallic surfaces, Surf. Sci. 604 (2010) 1845–1853.
[4] C.Y. Niu, J. Jiao, B. Xing, G.C. Wang, X.H. Bu, Reaction mechanism of methanol decomposition on pt-based model catalysts: a theoretical study, J. Comput. Chem. 31 (2010) 2023–2037.
[5] E. Antolini, J.R.C. Salgado, E.R. Gonzalez, The methanol oxidation reaction on platinum alloys with the first row transition metals. The case of Pt-Co and –Ni alloy electrocatalysts for DMFCs: a short review, Appl. Catal. B: Environ. 63 (2006) 137–149.
[6] A. Serov, T. Nedoseykina, O. Shvachko, C. Kwak, Effect of precursor nature on the performance of palladium–cobalt electrocatalysts for direct methanol fuel cells, J. Power Sources 195 (2010) 175–180.
[7] S. Litster, G. McLean, PEM fuel cell electrodes, J. Power Sources 130 (2004) 61–76.
[8] J. Kua, W.A. Goddard III, Oxidation of methanol on 2nd and 3rd row group VIII transition metals (Pt, Ir, Os, Pd, Rh, and Ru): application to direct methanol fuel cells, J. Am. Chem. Soc. 121 (1999) 10928–10941.
[9] S.C. Yao, X. Tang, C.C. Hsieh, Y. Alyousef, M. Vladimer, G.K. Fedder, C.H. Amon, Micro-electro-mechanical systems (MEMS)-based micro-scale direct methanol fuel cell development, Energy 31 (2006) 636–649.
[10] P. Hernández-Fernández, M. Montiel, P. Ocón, J.L.G. Fierro, H. Wangc, H.D. Abruña, S. Rojas, Effect of Co in the efficiency of the methanol electrooxidation reaction on carbon supported Pt, J. Power Sources 195 (2010) 7959–7967.
[11] P. Hirunsit, P.B. Balbuena, Surface atomic distribution and water adsorption on Pt-Co alloys, Surf. Sci. 603 (2009) 912–920.
[12] J.L. Park, M.G. Kim, Y.W. Jun, J.S. Lee, W.R. Lee, J. Cheon, Characterization of superparamagnetic "Core–Shell" nanoparticles and monitoring their anisotropic phase transition to ferromagnetic "Solid Solution" nanoalloys, J. Am. Chem. Soc. 126 (2004) 9072–9078.

[13] Z.T. Zhang, D.A. Blom, Z. Gai, J.R. Thompson, J. Shen, S. Dai, High-yield solvothermal formation of magnetic CoPt alloy nanowires, J. Am. Chem. Soc. 125 (2003) 7528–7529.
[14] Y.D. Qian, W. Wen, P.A. Adcock, Z. Jiang, N. Hakim, M.S. Saha, S. Mukerjee, PtM/C catalyst prepared using reverse micelle method for oxygen reduction reaction in PEM fuel cells, J. Phys. Chem. C 112 (2008) 1146–1157.
[15] J.C. Sotelo, J.M. Seminario, Biatomic substrates for bulk-molecule interfaces: the PtCo-oxygen interface, J. Chem. Phys. 127 (2007) 244706/1–244706/13.
[16] M. De Santis, R. Baudoing-Savois, P. Dolle, M.C. Saint-Lager, Chemical ordering in the first stages of Co-Pt film growth on Pt(111), Phys. Rev. B 66 (2002) 085412/1–085412/7.
[17] A. Stassi, I. Gatto, A. Saccá, A. Patti, G. Monforte, V. Baglio, A.S. Aricó, Design of supported PtCo electrocatalysts for PEMFCS, ECS Trans. 69 (2015) 263–272.
[18] J. Greely, M. Mavrikakis, A first-principles study of methanol decomposition on Pt(111), J. Am. Chem. Soc. 124 (2002) 7193–7201.
[19] J. Greely, M. Mavrikakis, Competitive paths for methanol decomposition on Pt(111), J. Am. Chem. Soc. 126 (2004) 3910–3919.
[20] W. Luo, A. Asthagiri, Density functional theory study of methanol steam reforming on Co(0001) and Co(111) surfaces, J. Phys. Chem. C 118 (2014) 15274–15285.
[21] F. Mehmood, J. Greeley, P. Zapol, L.A. Curtiss, Comparative density functional study of methanol decomposition on Cu_4 and Co_4, J. Phys. Chem. C 114 (2010) 14458–14466.
[22] Z. Jiang, B. Wang, T. Fang, A theoretical study on the complete dehydrogenation of methanol on Pd(100) surface, Appl. Sur. Sci. 364 (2016) 613–619.
[23] X.K. Gu, W.X. Li, First-principles study on the origin of the different selectivities for methanol steam reforming on Cu(111) and Pd(111), J. Phys. Chem. C 114 (2010) 21539–21547.
[24] Z. Jiang, S. Guo, T. Fang, Theoretical investigation on the dehydrogenation mechanism of CH_3OH on Cu(100) surface, J. Alloys Compd. 698 (2017) 617–625.
[25] J. Greely, M. Mavrikakis, Methanol decomposition on Cu(111): a DFT study, J. Catal. 208 (2002) 291–300.
[26] A.S. Moura, J.L.C. Fajín, A.S.S. Pinto, M. Mandado, M.N.D.S. Cordeiro, Competitive paths for methanol decomposition on ruthenium: a DFT study, J. Phys. Chem. C 119 (2015) 27382–27391.
[27] T.H. Upton, Theoretical studies of decomposition of methanol on Ni(100), J. Vacuum Sci. Technol. 20 (1982) 527–531.
[28] W.K. Chen, S.H. Liu, M.J. Cao, Q.G. Yan, C.H. Lu, Adsorption and dissociation of methanol on Au(111) surface: a first-principles periodic density functional study, J. Mol. Struct. Theochem. 770 (2006) 87–91.
[29] O. Skoplyak, C.A. Menning, M.A. Barteau, J.G. Chen, Experimental and theoretical study of reactivity trends for methanol on Co/Pt (111) and Ni/Pt (111) bimetallic surfaces, J. Chem. Phys. 127 (2007) 114707/1–114707/11.
[30] Y. Huang, Z.-X. Chen, Density functional investigation of the methanol dehydrogenation on Pd-Zn surface alloy, Langmuir 26 (2010) 10796–107802.
[31] J. Ye, C. Liu, Q. Ge, A DFT study of methanol dehydrogenation on the PdIn(110) surface, Phys. Chem. Chem. Phys. 14 (2012) 16660–16667.
[32] R.K. John, R. Karsten, S. Matthias, Alloy surface segregation in reactive environments: first-principles atomistic thermodynamics study of Ag3Pd(111) in oxygen atmospheres, Phys. Rev. B 77 (2008) 075437/1–075437/12.
[33] D. Yuan, X. Gong, R. Wu, Decomposition pathways of methanol on the PtAu(111) bimetallic surface: a first- principles study, J. Chem. Phys. 128 (2008) 064706/1–064706/5.
[34] N. Gabaldon-Limas, T.A. Manz, Introducing DDEC6 atomic population analysis: part 2. Computed results for a wide range of periodic and nonperiodic materials, RSC Adv. 6 (2016) 45727–45747.
[35] T.A. Manz, N. Gabaldon-Limas, Introducing DDEC6 atomic population analysis: part 1. Charge partitioning theory and methodology, RSC Adv. 6 (2016) 47771–47801.
[36] T.A. Manz, N. Gabaldon-Limas, Chargemol Program for Performing DDEC Analysis Version 3 4.4, 2016, ddec.sourceforge.net.
[37] S. Koh, J. Leisch, M.F. Toney, P. Strasser, Structure-activity-stability relationship of Pt-Co alloy electrocatalyst in gas-diffusion electrode layers, J. Phys. Chem. C 111 (2007) 3744–3752.
[38] S. Koh, C. Yu, P. Mani, R. Srivastava, P. Strasser, Activity of ordered and disordered Pt-Co alloy phases for the electroreduction of oxygen in catalysts with multiple coexisting phases, J. Powers Sources 172 (2007) 50–56.
[39] A. Stassi, I. Gatto, G. Monforte, V. Baglio, E. Passalacqua, V. Antonucci, A.S. Aricó, The effect of thermal treatment on structure and surface composition of PtCo electro-catalysts for application in PEMFCs operating under automotive conditions, J. Power Source 208 (2012) 35–45.
[40] L. Xiong, A. Manthiram, Effect of atomic ordering on the catalytic activity of carbon supported PtM (M = Fe, Co, Ni, and Cu) alloys for oxygen reduction in PEMFCs, J. Electrochem. Soc. 152 (2005) A697–A702.
[41] W.B. Pearson, A Handbook of Lattice Spacings and Structures of Metals and Alloys, Pergamon, Oxford, U.K, 1964, pp. 1958–1967.
[42] A. Dannenberg, M.E. Gruner, A. Hucht, P. Entel, Surface energies of stoichiometric FePt and CoPt alloys and their implications for nanoparticle morphologies, Phys. Rev. B 80 (2009) 245438/1–245438/15.
[43] G. Kresse, J. Hafner, Ab initio molecular dynamics for liquid metals, Phys. Rev. B 47 (1993) 558–561.
[44] G. Kresse, J. Furthmüller, Efficient iterative schemes for ab initio total-energy calculations using a plane-wave basis set, Phys. Rev. B 54 (1996) 11169–11186.
[45] G. Kresse, J. Furthmüller, Efficiency of ab-initio total energy calculations for metals and semiconductors using a plane-wave basis set, Comput. Mater. Sci. 6 (1996) 15–50.
[46] P.E. Blöchl, Projector augmented-wave method, Phys. Rev. B: Condens. Matter Mater. Phys. 50 (1994) 17953–17979.
[47] G. Kresse, D. Joubert, From ultrasoft pseudopotentials to the projector augmented-wave method, Phys. Rev. B: Condens. Matter Mater. Phys. 59 (1999) 1758–1775.
[48] J. Perdew, J.A. Chevary, S.H. Vosko, K.A. Jackson, M.R. Pederson, D.J. Singh, C. Fiolhais, Atoms, molecules, solids, and surfaces: applications of the generalized gradient approximation for exchange and correlation, Phys. Rev. B 46 (1992) 6671–6687.
[49] H.J. Monkhorst, J.D. Pack, Special points for Brillouin-zone integrations, Phys. Rev. B 13 (1976) 5188–5192.
[50] P. Bechthold, S. Ardenghi, V. Cardoso Schwindt, E.A. González, P.V. Jasen, V. Orazi, M.E. Pronsato, A. Juan, Benzene adsorption on PtCo(111): a DFT study, Appl. Surf. Sci. 282 (2013) 17–24.
[51] S. Grimme, Semiempirical GGA-type density functional constructed with a long-range dispersion correction, J. Comput. Chem. 27 (2006) 1787–1799.
[52] R. Hoffmann, Solid & Surface: A Chemist's View of Bonding in Extended Structures, 1st ed., Wiley-VCH, New York, 1989.
[53] R. Dronskowski, Computational Chemistry of Solid State Materials: A Guide for Materials Scientists, Chemists, Physicists and Others, Wiley-VCH, Weinheim, 2005.
[54] R.F.W. Bader, Atoms in Molecules – A Quantum Theory, Oxford University Press, Oxford, 1990.
[55] V. Orazi, J.S. Ardenghi, P. Bechthold, P.V. Jasen, M.E. Pronsato, E.A. González, DFT study of benzene and CO co-adsorption on PtCo(111), Appl. Surf. Sci. 289 (2014) 502–510.
[56] B. Sexton, Methanol decomposition on platinum (111), Surf. Sci. 102 (1981) 271–281.
[57] P. Gazdzicki, P. Uvdal, P. Jakob, Adsorption of intact methanol on Ru(0001), J. Chem. Phys. 130 (2009) 224703/1–224703/9.
[58] A. Bigotto, V. Galasso, G. de Alti, Infrared spectra and normal vibrations of cobalt(II), nickel(II) and palladium(II) complexes with N, N'-ethylenebis(acetyhetoneimine), Spectrochim. Acta 28A (172) (2017) 1581–1591.